AAS 15-293

2D CONTINUITY EQUATION METHOD FOR SPACE DEBRIS CLOUD COLLISION ANALYSIS

Francesca Letizia[*], Camilla Colombo[†], and Hugh G. Lewis[‡]

Small fragments are rarely included in the evolution of the debris population as their number is so large that the computational time would become prohibitive. However, they also can be dangerous to operational satellites, so it is important to study their contribution to the collision probability. This work proposes an analytical method to propagate fragment clouds, whose evolution under the effect of drag is studied on the space defined by the semi-major axis and the eccentricity. This approach provides an analytical expression of the cloud density that can be translated into a quick estimation of the collision probability.

INTRODUCTION

Around the Earth there are more than ten million objects larger than 1 mm that can interfere with other orbiting spacecraft. In particular, objects larger than 1 cm are considered massive enough to seriously damage or even destroy a satellite in case of collision.[1] The traditional piece-by-piece approach to study the evolution of debris objects cannot be applied to small fragments because their number is so large that the computational time would be prohibitive. For this reason, current debris model treat small fragments by sampling their population or by defining some *representative objects*,[2] whose trajectories are propagated and used to compute the resulting collision probability. In a previous work,[3] we proposed an alternative method where the small fragments are modelled in terms of their spatial density, whose evolution in time can be obtained thanks to the continuity equation approach for propagation proposed by McInnes.[4] The applicability of the method was discussed considering the evolution of a cloud of debris fragments generated by a collision and it was applied to compute the resulting collision probability in several scenarios.

Summarizing, the collision is simulated through a breakup model;[5,6] then, the orbital parameters of the generated fragments are numerically propagated[7,8] until they form a band around the Earth, because of the effect of perturbations;[9] at this moment, a continuous function is defined to describe the fragment spatial density and its evolution with time is obtained through the application of the continuity equation. Finally, the collision probability for a spacecraft crossing the cloud is computed applying the analogy with the kinetic theory for gas.

This approach offers two main advantages:

- the fragment cloud is studied as a whole in terms of its density, which can then be directly used to assess the collision probability due to the fragmentation under analysis;

[*]PhD candidate, Astronautics Research Group, University of Southampton, UK, SO17 1BJ, f.letizia@soton.ac.uk
[†]Lecturer, PhD, Astronautics Research Group, University of Southampton, UK, SO17 1BJ, currently Marie Curie Research Fellow at Politecnico di Milano, Italy, camilla.colombo@polimi.it
[‡]Senior Lecturer, PhD, Astronautics Research Group, University of Southampton, UK, SO17 1BJ, h.g.lewis@soton.ac.uk

- the formulation with the continuity equation admits an analytical solution if only the drag effect is considered, obtaining a considerable reduction in the computation time required to study a fragmentation event.

This last point, however, requires also other hypotheses on the cloud evolution such as the assumption that all the fragments are on quasi-circular orbits: it was observed that this hypothesis is acceptable only at altitudes equal and higher than $800\,\mathrm{km}$, whereas, at lower altitudes, the effect of the eccentricity needs to be considered.[10]

For this purpose, the continuity equation approach was extended to a 2D formulation,[11] able to take into account the initial distribution in eccentricity of the fragments in the cloud. With this formulation, the evolution of the cloud is not studied any more in a physical space, but in the phase space defined by the semi-major axis a and the eccentricity e, improving the accuracy of the method. In the following, the formulation of the 2D approach to model the density evolution through the continuity equation will be described; then, it will be discussed how the information on the distribution of the fragments in semi-major axis and eccentricity can be used to estimate the average relative velocity between the cloud and a target spacecraft crossing it. The validation procedure for the velocity estimation will be described in detail and, finally, an application scenario for the proposed method will be discussed.

2D APPROACH FOR THE DENSITY

The evolution of the fragment spatial density can be obtained through the continuity equation, a well-known equation of fluid-dynamics. In that field it is used to connect the evolution of density and velocity in a fluid. Similarly, it can be used in astrodynamics to describe the effect of different forces (e.g. atmospheric drag, Poynting-Robinson drag) on a set of orbiting objects such as pieces of interplanetary dust,[12] nanosatellites,[13] high area-to-mass objects[14] and space debris.[4] The general expression for the continuity equation is

$$\frac{\partial n}{\partial t} + \nabla \bullet \mathbf{f} = \dot{n}^{+} - \dot{n}^{-} \tag{1}$$

where n is the spatial density, $\nabla \bullet \mathbf{f}$ models slow/continuous phenomena and $\dot{n}^{+} - \dot{n}^{-}$ fast discontinuous events.

In the current application, the continuity equation is used to model the effect of atmospheric drag on a set of fragments produced by a collision or an explosion. Therefore, $\dot{n}^{+} - \dot{n}^{-} = 0$ as no discontinuous events are considered; $\nabla \bullet \mathbf{f}$ should instead model the flux of objects due to drag. In general, $\mathbf{f}$ may be a function of all six orbital elements of the fragments, but, as anticipated, the analytical propagation is applied only when the fragments have formed a band around the Earth. The spreading of the fragments from the initial dense configuration around the fragment location is driven by two factors:

1. the breakup distributes the energy differently among the fragments, meaning that just after the fragmentation all the fragments have the same initial position, but different velocities and, therefore, different orbital energies;

2. the Earth's oblateness causes the fragment orbits to rotate with a precession rate that depends on the fragment orbital parameters and that is, therefore, different among the fragments in the cloud.

As a result,

1. the true anomaly ν of the fragments is randomized (i.e., it is uniformly distributed across all its domain) in a few orbits,
2. the argument of the perigee ω and the longitude of the ascending node Ω are randomized too within some months from the fragmentation.[15]

Therefore, ν, ω, Ω can be excluded from the dependence of $\mathbf{f}$. With the hypothesis of a non-rotating atmosphere, the dependence on the inclination i can also be removed.

At this point, $\mathbf{f}$ can be written as a vector field with two components

$$\mathbf{f} = n(a, e; t) \begin{pmatrix} v_a(a, e; t) \\ v_e(a, e; t) \end{pmatrix} \tag{2}$$

where v_a and v_e are, respectively, the rate of variation of the semi-major axis a and the one of the eccentricity e caused by drag. In this work, they are obtained from King-Hele's expression[7] for the variation of the orbital parameters in one orbit, for orbits with eccentricity between 0.01 and 1:

$$\Delta a = -2\pi \frac{c_D A}{M} a^2 \rho_H \exp\Big(-\frac{a - R_H}{H}\Big)\Big[I_0 + 2eI_1 + O(e^2)\Big] \tag{3}$$

$$\Delta e = -2\pi \frac{c_D A}{M} a \rho_H \exp\Big(-\frac{a - R_H}{H}\Big)\Big[I_1 + \frac{e}{2}(I_0 + I_2) + O(e^2)\Big]; \tag{4}$$

where c_D, A, M are respectively the fragment drag coefficient, its area and its mass; ρ_H, R_H, H are the reference density, the reference altitude and the scale height, coming from the exponential model of the atmosphere. I_n indicates the modified Bessel function of the first kind and order n with argument $z = ae/H$.

By wrting

$$f(a, e, H) = I_0 + 2eI_1 + O(e^2) \tag{5}$$

$$g(a, e, H) = I_1 + \frac{e}{2}(I_0 + I_2) + O(e^2), \tag{6}$$

introducing the parameter ε

$$\varepsilon = \frac{c_D A}{M} a \rho_H \tag{7}$$

and dividing Eqs. (3) and (4) by the orbital period $T = 2\pi\sqrt{\mu/a^3}$, the expression of the velocities is obtained

$$v_a = -\sqrt{\mu a}\varepsilon \exp\left(-\frac{a - R_H}{H}\right) f(a, e, H) \tag{8}$$

$$v_e = -\sqrt{\frac{\mu}{a}}\varepsilon \exp\left(-\frac{a - R_H}{H}\right) g(a, e, H). \tag{9}$$

The expressions of the velocities are further simplified to obtain an explicit analytical solution

$$v_a = -\sqrt{\mu R_H}\varepsilon \exp\left(-\frac{a - R_H}{H}\right) f(R_H, \tilde{e}(a), H) \tag{10}$$

$$v_e = 0 \tag{11}$$

where $\tilde{e}(a)$ expresses a reference value of the eccentricity for each semi-major axis. This relationship is obtained from the distribution of the fragments at the initial instant of the analytical propagation, when the band is formed. A detailed discussion on the reasons for this approximation and an evaluation of its accuracy is given in Letizia et al.[11] This approximation can be summarized by saying that finding an analytical solution requires decoupling the equations for a and e. This can be done, for example, assuming that the eccentricity is constant as in Eq. (11) and using the information on the initial eccentricity distribution to correct the variation rate of the semi-major axis. As will be shown later with an example, this allows an improvement in the accuracy of the analytical propagation compared to the 1D formulation and the extension of the applicability of the method.[11]

Given the expression in Eq. (11), the continuity equation can be solved adopting the method of characteristics obtaining the following expression for the density

$$n(a, e; t) = n_0(a_i, e_i) \frac{v_a(a_i)}{v_a(a)} \tag{12}$$

where n_0 is the initial density at the band formation and a_i, e_i are two functions obtained by inverting the characteristics of the system at the initial time:

$$a_i(a, t) = -H \log \left[\exp\left(\frac{a - R_H}{H} \right) + \varepsilon \left(R_H + \tilde{e}(a), H \right) \frac{\sqrt{R_H}}{H} t \right] \tag{13}$$

$$e_i(e, t) = e. \tag{14}$$

Thanks to Eq. (12) the value of the density in the phase space at any time is known once the initial condition is given. Fig. 1 shows the value of the density in the phase space at the band formation and after 1000 days for a fragmentation at 700 km.

The information in the phase space needs to be mapped into the real physical space to be used to compute the collision probability for a spacecraft crossing the cloud. This passage requires an expression able to translate the information about the orbital parameters into a distribution in spatial density. In contrast to the previous version of the method,[11] here Kessler's[16] expressions for the spatial density are used because, similarly to what was found for the 1D case,[17] they improve the description of the peak in the fragment distribution. According to Kessler,[16] the spatial density at a point, with distance r and latitude β, inside the fragment cloud is equal to

$$S(r, \beta) = s(r) w(\beta) = \frac{1}{4\pi^2 r a \sqrt{[r - a(1-e)][a(1+e) - r]}} \frac{2}{\pi \sin \alpha \cos \beta} \tag{15}$$

where $\cos \alpha = \cos i / \cos \beta$.

As explained in detail in Letizia et al.,[17] the dependence on the latitude is neglected here because β evolves on a much faster time scale than the one used to follow the cloud evolution. For this reason, an average value of $w(\beta)$ across the band is used. Therefore, only

$$s(r) = \frac{1}{4\pi^2 r a \sqrt{[r - a(1-e)][a(1+e) - r]}} \tag{16}$$

is used to pass from the formulation in (a, e) to the fragment spatial density. Observe here that Eq. (16) was written specifically for cases where ν, ω, Ω are randomized, and only a and e are known. Considering again Fig. 1, Eq. (16) is applied to all the domain in (a, e) to obtain the spatial density at different altitudes and times as shown in Fig. 2for a fragmentation at 700 km.

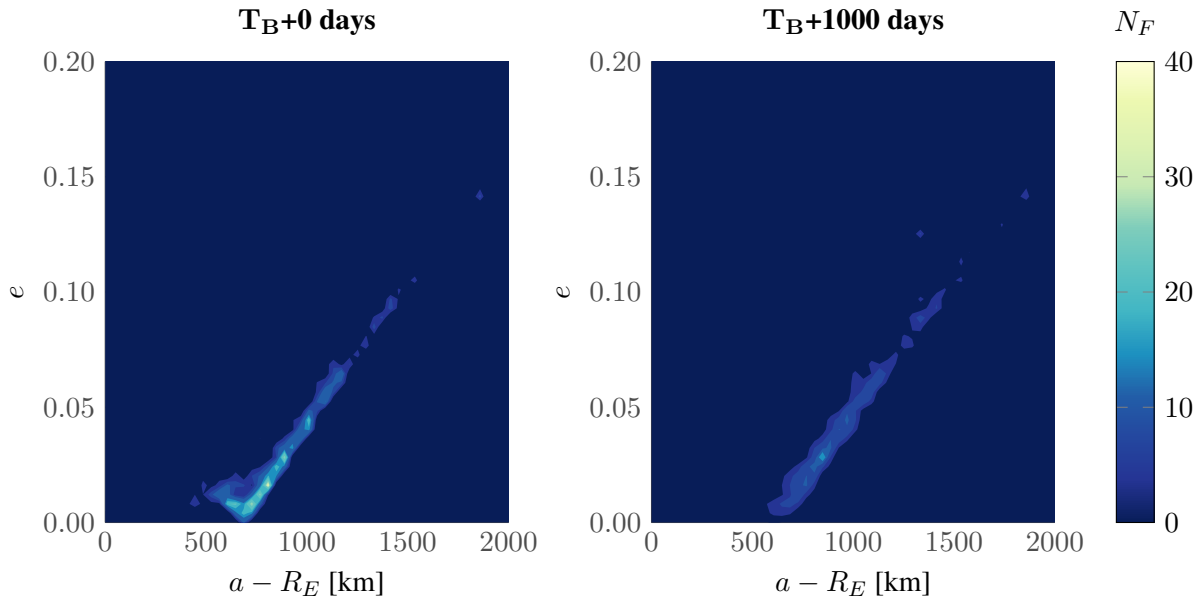

Figure 1: Visualization of cloud density at the band formation (T_B = 92 days) and after 1000 days expressed in number of fragments N_F in any cell of the (a, e) domain, which is discretized by a grid of 100 points along both dimensions. The represented value of the cloud density is the one obtained with the analytical expression in Eq. (12).

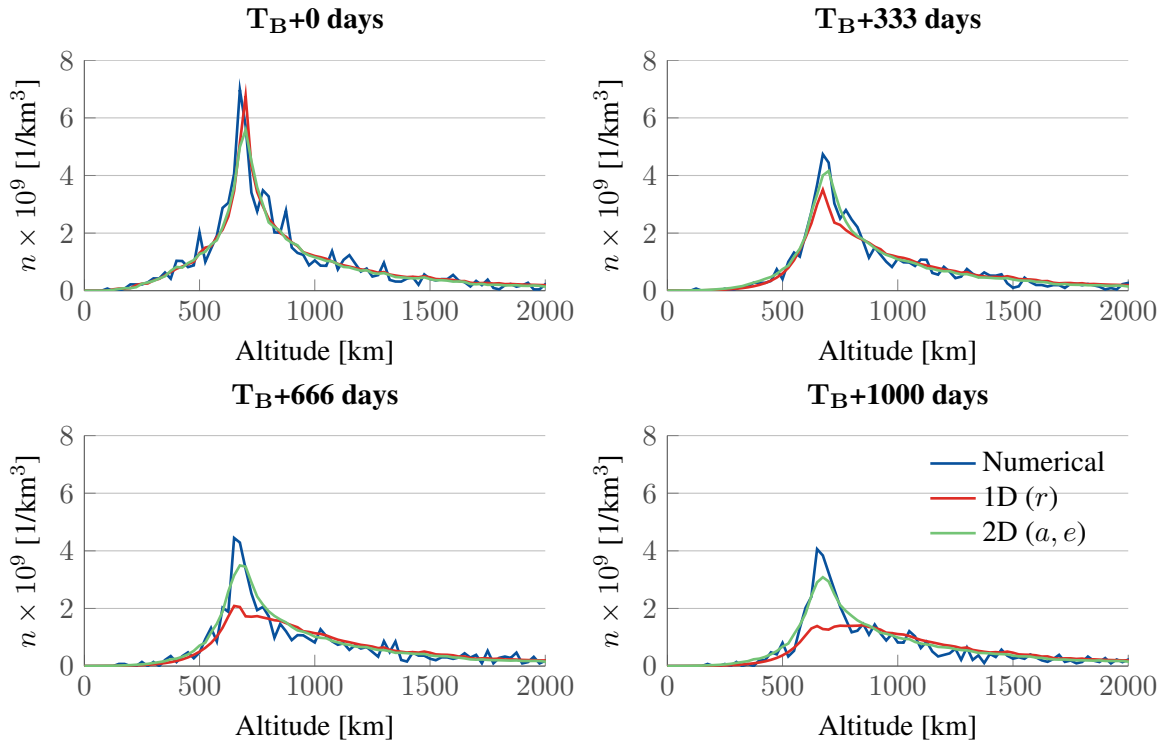

Figure 2: Density profile evolution for a fragmentation at 700 km in four instants after the band formation (T_B = 92 days).

The density obtained with the analytical method is compared with the one obtained propagating with a numerical method the trajectory of each fragment and checking their altitude. The value of the density for the numerical propagation is computed by separating the altitude domain into bins with width equal to $25\,\text{km}$. The value of the spatial density is then obtained dividing the fragment number in each bin by the volume of the spherical shell corresponding to each bin. The analytical method, instead, provides directly a result expressed in spatial density with units km $^{-3}$.

In 1000 days after the time of the band formation T_B, the 1D formulation of the continuity approach is no longer able any more to represent the fragment distribution and, in particular, the distribution peak is not captured by the analytical propagation. Instead, the 2D propagation provides a more accurate description of the fragment distribution: the peak location is well captured and the error on its height is halved compared to the 1D propagation.

For what concerns the computational aspect of the method, Eq. (16) was implemented in the code considering the four simplified expressions derived by Kessler.[16] These four simplified expressions hold when Eq. (16) is used to compute the fragment spatial density between two close values of altitude (r and r'), so that

$$\Delta r = r' - r \quad \bar{r} = \frac{r' + r}{2} \quad \Delta r \ll \bar{r}.$$

This is true in our case if the density is evaluated on an array of altitude values with a fine spacing. For example, using the same bin width adopted for the numerical results ($\Delta h = 25\,\text{km}$), $\Delta h / R_F \approx 0.0035$ for the case where the fragmentation occurs at $R_F = R_E + 700\,\text{km}$ as in the example shown in Figs. 1 and 2. In Kessler's original formulation the choice about which expression to use is based on the comparison between the *target* altitude (r) and the orbital parameters of the *dispersed* object. In details, the possible combinations are

1. $r > a(1-e)$ and $r' < a(1+e)$
2. $r \leq a(1-e)$ and $r' \leq a(1+e)$
3. $r \geq a(1-e)$ and $r' \geq a(1+e)$
4. $r \leq a(1-e)$ and $r' \geq a(1+e)$.

In the current application, given the altitude r where we want to compute the density, the domain in (a, e) can be easily split into the four zones identified by Kessler.[16] Fig. 3 shows an example of this process for a target altitude equal to $800\,\text{km}$. With this approach, the combinations of (a, e) that affect a given altitude can be identified immediately. Moreover, purely from a computational point of view, this subdivision of the domain exploits the capabilities of software such as MATLAB for working efficiently with matrices. Finally, in the previous version of the method[11] the transformation from the phase space (a, e) to the physical space (r) produced as output the distribution of the spatial density with altitude or, in other words, for each point in the domain (a, e) its impact on the whole r-domain was evaluated. Now, instead, the implementation associated with Fig. 3 switches the point of view to evaluate how a given value in r is affected by the distribution in (a, e). This approach results in improved convenience in terms of computational time when the method is used to compute the density at a specific altitude many times as in the case of the analysis of the collision probability for a target crossing a fragment cloud.

2D APPROACH FOR THE VELOCITY

The propagation method outlined in the previous Section can be used to obtain an efficient estimation of the fragment spatial density associated with a fragmentation event in Low Earth Orbit

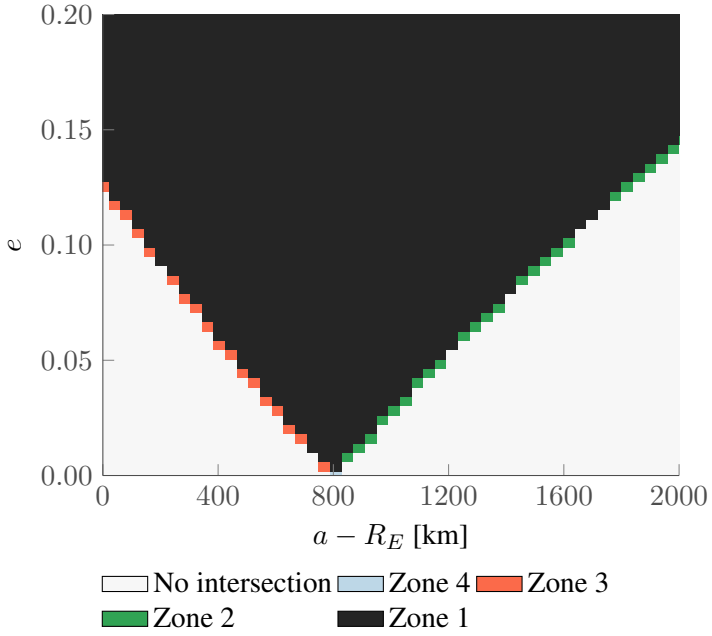

Figure 3: Subdivision of the integration domain into the areas where the simplified expressions from Kessler apply.

(LEO) and to assess the collision probability for spacecraft in the proximity of the fragmentation location.

Applying the traditional analogy with the gas kinetic theory, the cumulative collision probability can be written as

$$p_c = 1 - \exp\left(-N\right) \tag{17}$$

where N is the average number of collisions in a time interval Δt

$$N = n\Delta v \sigma \Delta t \tag{18}$$

with n the cloud spatial density, Δv the average relative speed between the target and the fragments, and σ the collisional cross sectional area. In the current application, the fragments have a much smaller cross sectional area than the target, so σ is simply set equal to the target area. The spatial density can be obtained from the analytical propagation as described in the previous section.

The relative velocity between the target and the fragments, instead, needs to be estimated from the information available from the propagation of the target and of the fragments. In previous works based on the 1D propagation,[17,18] it was considered to depend only on the target altitude, assuming that both the target and the fragments are on quasi-circular orbits, and that their velocities are always orthogonal. These hypotheses can be used together with the law of cosines to write the magnitude of the relative velocity Δv between the target and a fragment

$$\Delta v^2 = v_T^2 + v_F^2 - 2 v_T v_F \cos\phi \tag{19}$$

where v_T is the magnitude of the target velocity, v_F is the one of the fragment velocity and ϕ is the

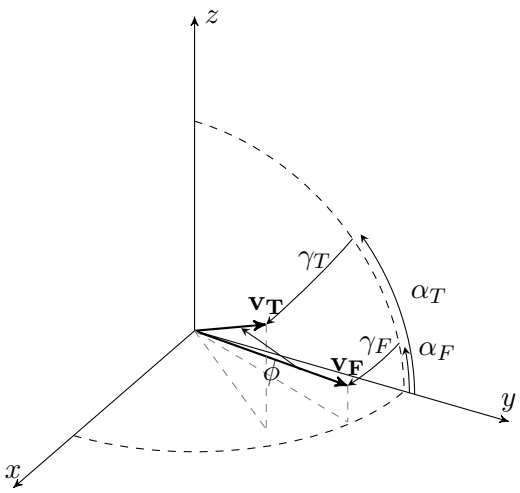

Figure 4: Definition of the angles between the velocity vectors according to Kessler.[16]

angle between the two vectors. The hypothesis on quasi-circular orbits can be expressed as

$$v_T \approx v_F \approx \sqrt{\frac{\mu}{r_T}},$$

where r_T is the target altitude. Assuming the vectors to be perpendicular leads obviously to $\cos\phi = 0$, so that

$$\Delta v = \sqrt{\frac{2\mu}{r}}. \tag{20}$$

The idea here is to understand how this estimation can be improved considering the additional information available from the 2D approach. Firstly, it is possible to observe that no approximation is required for the target velocity, which is given by the numerical propagation of the target trajectory. Secondly, we are interested in knowing the difference between the target and the fragment velocities in conditions where they can meet. Therefore, v_F can be estimated through the value of the orbital velocity at the target altitude (r_T)

$$v_F \approx \sqrt{2\mu\left(\frac{1}{r_T} - \frac{1}{2a_F}\right)},$$

where a_F is the fragment semi-major axis.

Also the angle ϕ can be estimated from the orbital parameters[16] solving the spherical triangle in Fig. 4

$$\cos\phi = \sin\gamma_T \sin\gamma_F + \cos\gamma_T \cos\gamma_F \cos\left(\alpha_T - \alpha_F\right) \tag{21}$$

where the subscript T refers to the target and F to the fragment. The two angles γ and α are defined respectively as

$$\cos^2\gamma = \frac{a^2(1-e^2)}{r(2a-r)} \tag{22}$$

$$\cos\alpha = \frac{\cos i}{\cos\beta} \tag{23}$$

where r and β are the altitude and the latitude where we would like to estimate ϕ, that is at the target location.

Considering all possible choices for the signs of γ and α, there are 16 possible combinations[16] that can be reduced to eight considering the property of symmetry of the trigonometric functions. These eight possible combinations can all be described by

$$\cos\phi = \pm\sin\gamma_T \sin\gamma_F \pm \cos\gamma_T \cos\gamma_F \cos\left(\alpha_T \mp \alpha_F\right) \tag{24}$$

where now the angles are always taken in absolute value. Out of the eight combinations, only four are compatible with the geometry of the problem. Note that, since no information is available on ν, ω, Ω is not possible to further reduce the number of solutions, except for simple planar, circular cases. Therefore, with this method the relative velocity between the target and a fragment is the average among the four possible values associated with the four possible values of ϕ.

To understand how to reduce Eq. (24) to only four possible solutions, it is convenient to consider a simplified case when the target is on a circular and planar orbit, and the fragment is on a circular orbit with the same radius as the target. In this case

$$\cos^2\gamma_T = 1 \quad \sin\gamma_T = 0 \quad \alpha_T = 0 \quad \alpha_F = \pm i_F$$

and

$$\cos\phi = \pm\cos i_F. \tag{25}$$

It is easy to observe that only one sign of $\cos\phi$ in Eq. (25) is admissible, depending on the direction of motion of the target and of the fragment along their orbits. For example, Fig. 5a shows the two vectors $\mathbf{v_T}$ and $\mathbf{v_F}$ on the yz-plane in the case that Ω_F = 0; the angle ϕ is equal to the inclination of the fragment orbit. This is true also for the case with $\Omega_F = \pi$ (shown in grey in Fig. 5a) and so, in this situation, the correct choice is the positive sign for $\cos\phi$ in Eq. (25).

Also relaxing the hypothesis on $i_T = 0$, it is possible to obtain a similar velocity diagram, as shown in Fig. 5b. In this case

$$\cos\phi = \pm\cos\left(i_T \mp i_F\right) \tag{26}$$

and also here only the positive sign is compatible with the problem geometry; the sign in the cosine, instead, captures the two possible values of ϕ due to the different possible values of Ω.

Therefore, the information on the inclination of target and fragment orbits can be used to decide the sign for $\cos\phi$

+ if they are both on direct or retrograde orbits (same direction of motion)

- otherwise.

The condition on the sign of $\cos\phi$ allows selecting the only four possible values for ϕ to estimate Δv.

In the following, for simplicity we will show only results for quasi-circular targets, so that the equation for ϕ is simplified into

$$\cos\phi = \pm\cos\gamma_F \cos\left(\alpha_T \mp \alpha_F\right), \tag{27}$$

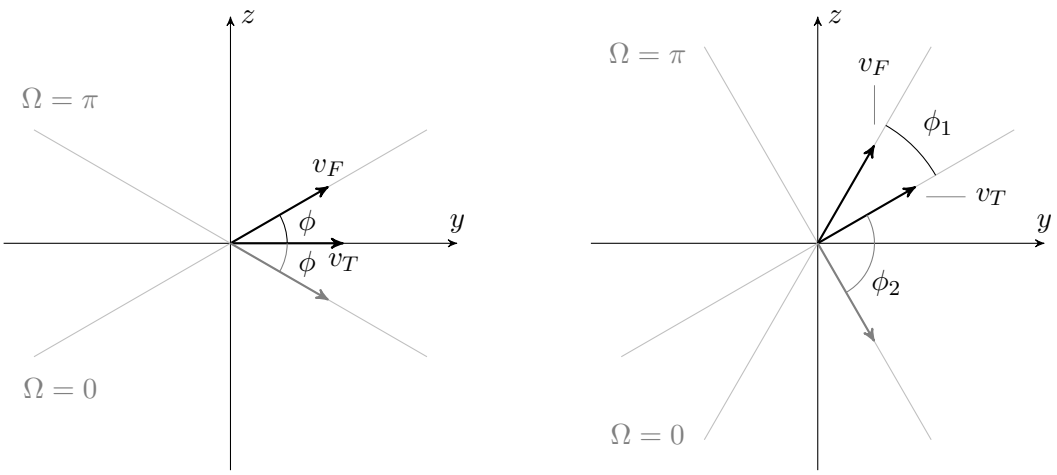

(a) Planar target orbit

(b) Non-planar target orbit

Figure 5: Velocity diagrams

which, as discussed before and shown in Fig. 5b, admits only two possible solutions.

The applications of these expressions to a debris cloud require some small modifications to consider two elements. Firstly, the value of the latitude β in a certain time instant is not representative of the entire the time step when this is much longer than one orbit. This is the case for the study of the collision probability on a time scale of some years, where following the target trajectory with a very fine time step (shorter than one orbit) would result in a unnecessary large computational effort. Therefore, the term $\cos(\alpha_T \mp \alpha_F)$ in Eq. (27) could be computed considering its mean value as

$$\cos(\alpha_T \mp \alpha_F) = \frac{\int_{-\beta_{\max}}^{\beta_{\max}} \cos\left[\arccos\left(\frac{\cos i_T}{\cos\beta}\right) \mp \arccos\left(\frac{\cos i_F}{\cos\beta}\right)\right] \mathrm{d}\beta}{2\beta_{\max}} \tag{28}$$

with $\beta_{\max} = \min(i_T, i_F)$. Secondly, in Kessler[16] the expressions are applied to a small number of objects*, so the value of the relative velocity is found as an average of all the possible values from Eq. (24). In our case there are, instead, thousands of objects with (Ω, ω) equally distributed among them. In this case, averaging among the extremes of the distribution leads to a systematic error because the relationship between the angle ϕ and the distributed angles (Ω, ω) is not linear. This was observed considering in particular the dependence of ϕ on the difference in the longitude of the ascending nodes $\Delta\Omega$ in the case of two circular orbits.† This case can be represented by the spherical triangle in Fig. 6 where A is the ascending node of the target orbit and B the ascending node of the fragment orbit. Therefore,

$$B = i_T \quad C = \pi - i_F;$$

also $a = \Delta\Omega$, so the spherical triangle can be solved with the law of cosines to find the angle A

$$A = \arccos\left[\sin B \sin C \cos a - \cos B \cos C\right] \tag{29}$$

$$= \arccos\left[\sin(i_T)\sin(i_F)\cos(\Delta\Omega) + \cos(i_T)\cos(i_F)\right] \tag{30}$$

*the eight outer moons of Jupiter

†We are assuming that the inclination i and the longitude of the ascending node Ω are the parameters that drive the value of ϕ because they define the difference in the two orbital planes.

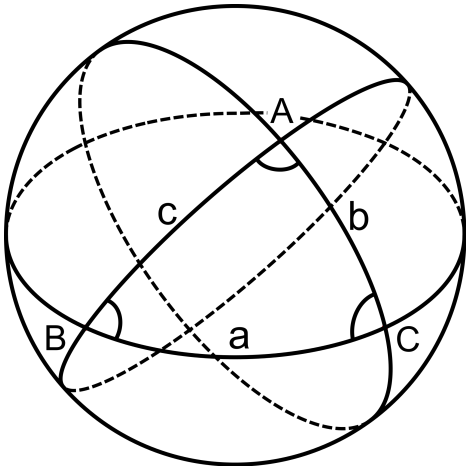

Figure 6: Generic spherical triangle.

Eq. (30) can be used to provide a unique value of ϕ for a given configuration of target and fragments in terms of their inclinations. In fact, given that Ω is uniformly distributed among the fragments

$$\bar{\phi} = \frac{\int_0^{\pi} \arccos\left[\sin\left(i_T\right)\sin\left(i_F\right)\cos\left(\Delta\Omega\right) + \cos\left(i_T\right)\cos\left(i_F\right)\right] \mathrm{d}\Delta\Omega}{\pi} \tag{31}$$

where the integration limits are set between 0 and π because the function is symmetrical with respect to the y-axis. Eq. (31) does not admit an analytical solution, so $\bar{\phi}$ is computed through numerical integration.

Moreover, the fragments are not on circular orbits, so Eq. (31) is used to compute $\overline{\Delta\alpha}$ in Eq. (27)

$$\cos\phi = \pm\cos\gamma_F \cos\overline{\Delta\alpha},$$

so γ_F is still used to take into account the effect of the eccentricity.

Combining the approximations for v_F and ϕ, it is possible to compute

$$\Delta v^2 = v_T^2 + v_F^2 - 2v_T v_F \cos\phi$$

for all the points in the (a, e) domain. The average value of Δv, which will then be used in Eq. (18) to estimate the collision probability, is finally obtained through a weighted average using the density as a weighting factor

$$\Delta\bar{v} = \frac{\iint n(a,e)\Delta v(a,e)\,\mathrm{d}a\mathrm{d}e}{\iint n(a,e)\,\mathrm{d}a\mathrm{d}e}. \tag{32}$$

The estimation is refined by considering which combinations of (a, e) actually correspond to orbits that intersect the target trajectory, similarly to what was explained for Fig. 3. A matrix $I(a, e)$ can be defined in the following way

$$I(a_j, e_k) = \begin{cases} 1, & \text{if } a_j(1-e_k) \leq r_T \leq a_j(1+e_k) \\ 0, & \text{otherwise} \end{cases}$$

and then Eq. (32) becomes

$$\Delta\bar{v} = \frac{\iint I(a,e)n(a,e)\Delta v(a,e)\,\mathrm{d}a\mathrm{d}e}{\iint I(a,e)n(a,e)\,\mathrm{d}a\mathrm{d}e}. \tag{33}$$

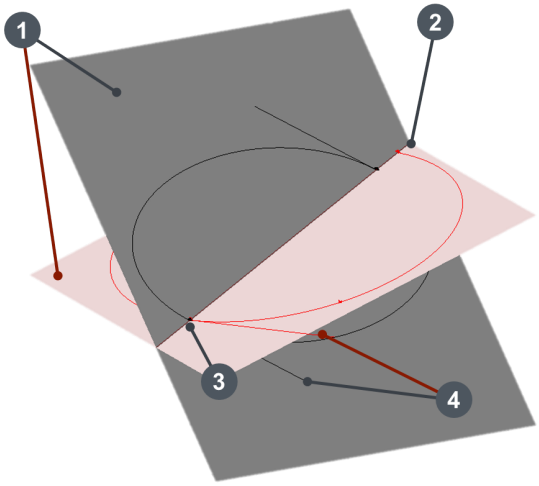

Figure 7: Sketch of the validation procedure.

VALIDATION OF THE VELOCITY ESTIMATION

Eq. (33) provides a fast method to estimate the average relative velocity between the target and the fragments once the target trajectory and the cloud density are known. On the other hand, some hypotheses were introduced to deal with the lack of information about the parameters ω and Ω. For this reason, the approach was validated adopting an independent, numerical procedure based on knowledge of all the orbital parameters both for the target and for the fragments.

The reference average velocity at any time of the analysis is computed with the following workflow (Fig. 7):

1. the orbital plane of the target is intersected by the orbital plane of each fragment
2. the line obtained from the intersection of the planes is used to find the intersections between the line itself and the orbits
3. the two pairs of points obtained are checked measuring their distance
4. if the distance is lower than a given threshold value (10 km in this case) the relative velocity between the target and the fragment at the intersection point is computed and stored
5. the average value among all the stored velocities is computed and used as reference value.

Additional details on the mathematical passages of the procedure are given in the Appendix.

The approach is similar to computation of the *Minimum Orbital Intersection Distance* (MOID), defined as "a measure for the distance between the orbits of an asteroid and of the Earth, not considering the positions that the bodies occupy in them".[19] In fact, also with the method here used to estimate the relative velocity, the check is not made on the current positions of target and fragments because, as discussed already for the latitude, comparing the target and the fragment positions at

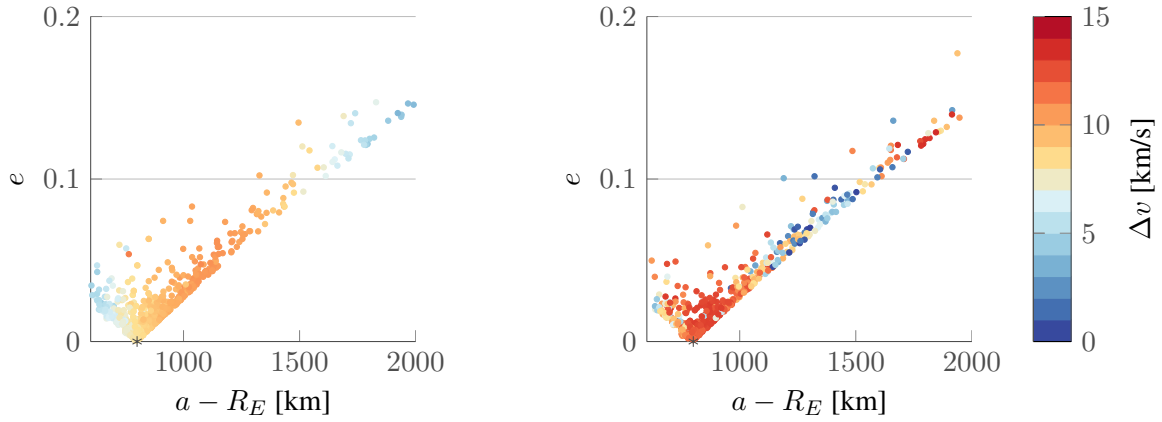

(a) F(30,800)T(60,800)

(b) F(60,800)T(60,800)

Figure 8: Relative velocity Δv_N distribution among the fragments with distance lower than 50 km at the band formation for two simulated cases. The cases are indicated with the notation F(i_F,$a_F - R_E$)T(i_T,$a_T - R_E$).

only one instant is not representative of the whole time step. In other words, this approach computes the relative velocity considering that if the orbits of two objects intersect, then the two objects will both be at the intersection point at a certain time.

The validation process was carried out for different combinations of target altitude and inclination with respect to the parent orbit from which the cloud is generated. The target mass and size were set considering the average values among possible targets;[20] in particular,

$$A_T = 11\,\mathrm{m}^2 \quad m_T = 2322\,\mathrm{kg}.$$

Some examples of the results obtained during the validation process are presented in Fig. 8, which shows the distribution of the relative velocity Δv among the fragments for different cases, indicated with the notation F(i_F,$a_F - R_E$)T(i_T,$a_T - R_E$). It is possible to observe how the value of Δv is affected by the inclination of the target orbit and by the one of the fragmentation orbit. While in Fig. 8a a dependence on the semi-major axis is visible, in Fig. 8b the value of Δv seems less correlated with the semi-major axis indicating that other parameters, such as the difference in the longitude of the ascending nodes, play a major role.

The results of the validation are shown in Fig. 9, which presents the *average* relative error on a five-year simulation for different combinations of the target and the fragment inclination. Similar simulations were done also varying the semi-major axis of the two orbits, but this parameter appears to have a very limited effect on the accuracy of the estimation.

The average relative error $\overline{\mathrm{err}}_{\mathrm{rel}}$ is here computed as

$$\overline{\mathrm{err}}_{\mathrm{rel}} = \frac{\int |\Delta v_A - \Delta v_N|\,\mathrm{d}t}{\int \Delta v_N\,\mathrm{d}t}, \tag{34}$$

where Δv_N is the estimation of the velocity obtained using the procedure outlined earlier in this section and Δv_A is the analytical estimation described in the previous section. Basically, Eq. (34) measures if the analytical approximation is able to capture the average value of the relative velocity,

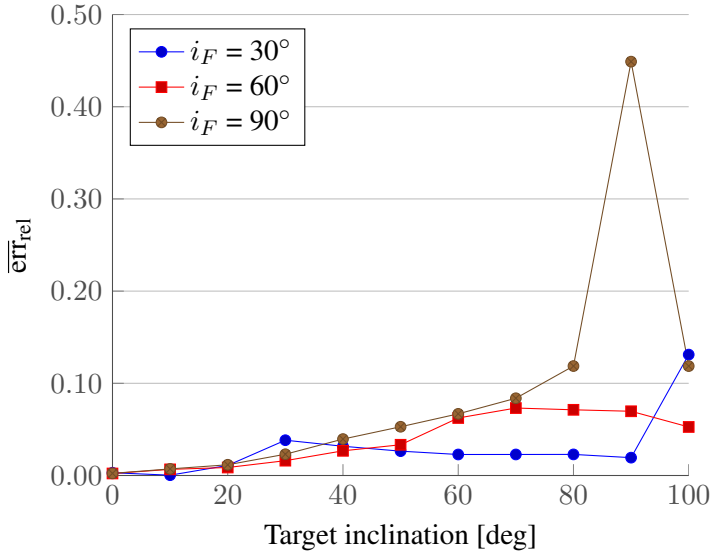

Figure 9: Average relative error for the analytical estimation of the relative velocity.

which is considered to be the most relevant parameter in a long-term study of the collision probability. It is possible to observe that, except for four cases close to $i_T = 90°$, the average relative error is below 10%, so the analytical estimation appears able to represent the average relative velocity between the target and the fragments.

Fig. 10 can be useful to better understand the numbers in Fig. 9. Fig. 10 represents the value of the reference relative velocity (in blue) and of the analytical estimation (in red) along the considered time window. In the first plot, Fig. 10a, the case F(30,800)T(60,800) with $\overline{\text{err}}_{\text{rel}} = 0.02$ is presented: the reference relative velocity oscillates with time because the target and the fragments have different inclination, and, therefore, they are subject to different precession rates of their orbital planes. For this reason and because Ω is not equally distributed among the fragments close to the target orbit, the average $\Delta\Omega$ between the target and the fragments changes with time. On the other hand, the analytical estimation changes much more slowly. In fact, considering the expressions in Eqs. (19) and (33), it is possible to observe that having removed the dependence on the latitude, $\overline{\Delta v}$ varies only following the (slow) evolution of the target orbital parameters and of the cloud density.

The second plot, Fig. 10b shows, instead, the case F(60,800)T(60,800) with $\overline{\text{err}}_{\text{rel}} = 0.06$: in this case target and fragments have the same inclination, so the oscillations are less defined than in the previous case. Fig. 11 shows the distribution of ϕ as a function of $\Delta\Omega$ for the case F(60,800)T(60,800) at $t = 500$ days. Each blue dot represents a fragment and the blue dashed line indicates the average ϕ among all fragments; the red dots represent, instead, the fragments with distance smaller than 10 km and also in this case the dashed line indicates the average ϕ obtained from this set of fragments. Finally, Eq. (30), the analytical expression for the dependence of ϕ on $\Delta\Omega$, is plotted in black and the average value, Eq. (31), is indicated with the dashed black line. It is possible to observe that, as expected, the fragments are distributed along the theoretical line in black; the dispersion across the line is due to the effect of the fragment ω, which is not described in Eq. (30).

From Fig. 9 the worst case appears to be F(90,800)T(90,800) as $\overline{\text{err}}_{\text{rel}} = 0.45$. The comparison

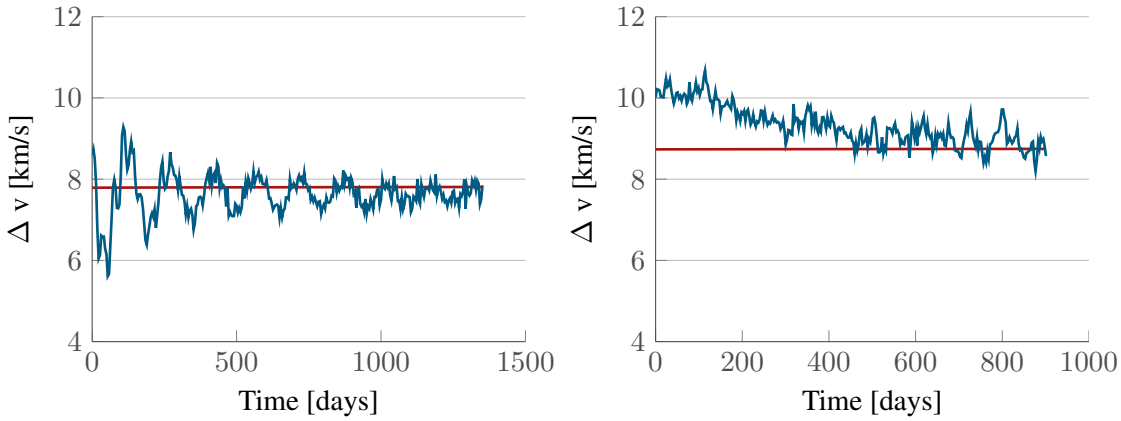

(a) F(30,800)T(60,800) with $\overline{\text{err}}_{\text{rel}} = 0.02$ (b) F(60,800)T(60,800) with $\overline{\text{err}}_{\text{rel}} = 0.06$

Figure 10: Comparison between the reference relative velocity Δv_N in blue and the analytical estimation Δv_A in red.

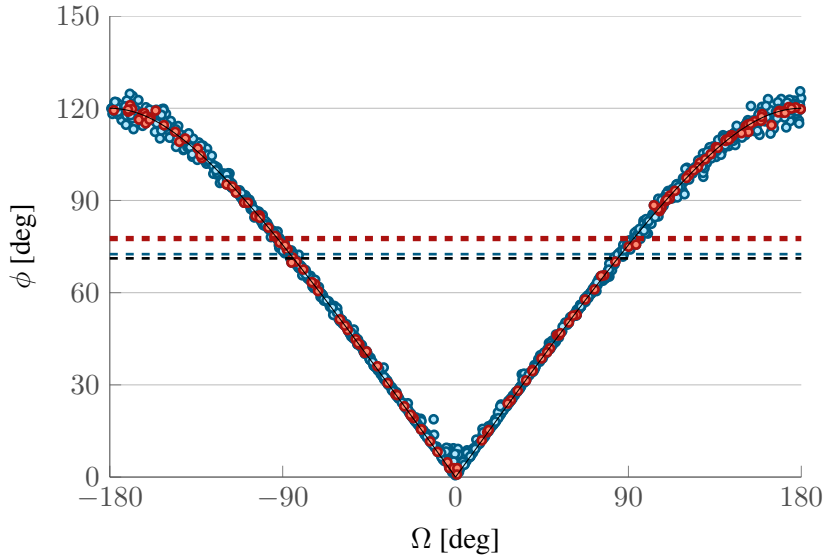

Figure 11: Distribution of ϕ as a function of $\Delta\Omega$ for the case F(60,800)T(60,800) at $t = 500$ days.

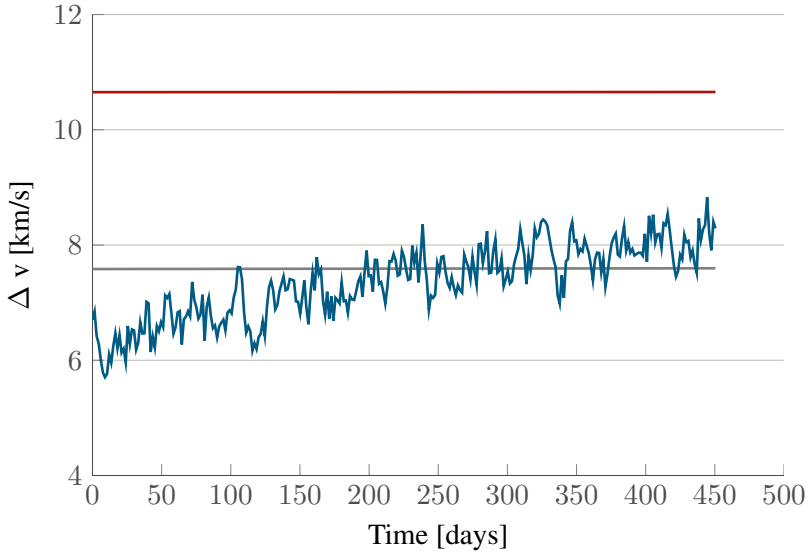

Figure 12: Comparison between the reference relative velocity Δv_N in blue and the analytical estimation Δv_A in red for the case F(90,800)T(90,800) with $\overline{\text{err}}_{\text{rel}} = 0.45$. The gray line represent the analytical estimation Δv_A obtained by averaging the extremes of the distribution with $\Delta\Omega$.

between the reference relative velocity and the analytical estimation is shown in Fig. 12, where the gray line refers to the estimation obtained by averaging the extremes of the distribution as in Kessler[16] instead of computing the integral mean as in Eq. (31). The average relative error for the grey line is much lower ($\overline{\text{err}}_{\text{rel}} = 0.03$), so this suggests that it should be possible to formulate an analytical expression able to estimate correctly the average relative velocity for any combination of i_T and i_F. This extension will be the object of future work.

COLLISION PROBABILITY COMPUTATION

Thanks to the analytical estimation of the relative velocity, we have now all the elements to compute the average number of collisions N in a time interval Δt as in Eq. (18)

$$N = n\Delta v\sigma\Delta t$$

and the resulting collision probability

$$p_c = 1 - \exp(-N).$$

As an example, the results for the case F(60,800)T(60,700) are shown. The considered debris cloud is formed by 2397 fragments, whose dynamics are studied for three years after the band formation T_B, which is equal to 286 days in this case. Fig. 13 shows the evolution of the cloud density in the ae-plane; the white vertical line represents the target altitude and the two inclined lines define the limits of the region on the ae-plane that contains the fragments that can affect the target. Fig. 14 shows instead the temporal evolution of the target altitude h_T, the fragment density at the target altitude n_T, the average relative velocity Δv and the collision probability p_c. It is possible to observe how n_T decreases in the first two years because during this period the fragments a low altitudes (left branch of the v-shaped distribution in Fig. 13) are removed by the effect of

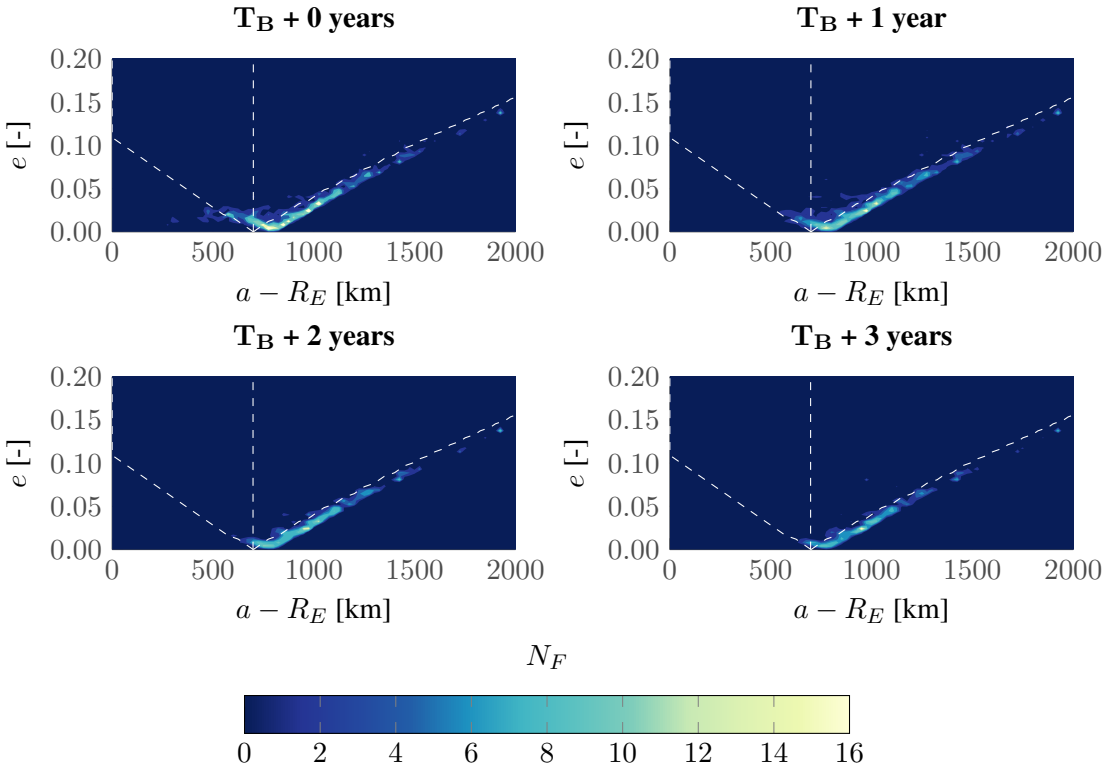

Figure 13: Evolution of the cloud density in the ae-plane for the case F(60,800)T(60,700).

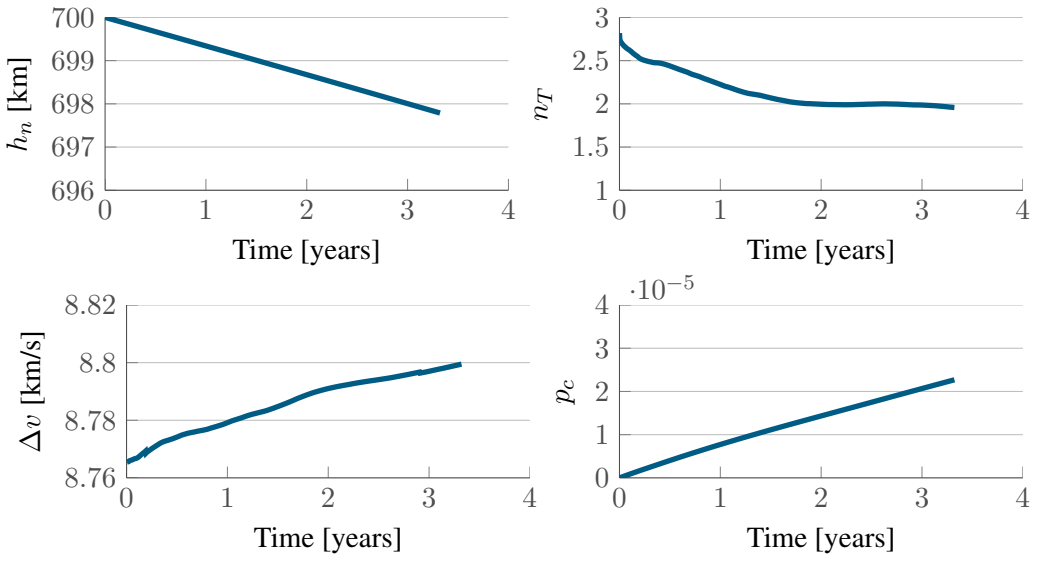

Figure 14: Temporal evolution of the target altitude h_T, the fragment density at the target altitude n_T, the average relative velocity Δv and the collision probability p_c.

drag. Afterwards, the density value is almost constant because the fragments that are still in orbit are less affected by drag. In the same time, the relative velocity increases as the target moves slowly to lower altitudes and the average semi-major axis increases. As a result, the collision probability grows with a slowly decreasing slope.

The result was obtained in 140.98 s on a PC with 8 CPUs at 3.40 GHz; most of the time was spent for the 2D analytical propagation (101.11 s): some options are currently under investigation to try to reduce this time by changing how the initial condition (n_0 in Eq. (12)) is translated across the domain. The estimation of the relative velocity is, instead, done in 3.57 s: this number is particularly interesting considering that the validation method described in the previous section (Fig. 7) requires 11.5 s for each time step.

For this reason, the analytical method based on the continuity equation and on the analytical estimation of the relative velocity appears to be an interesting approach to study many collision scenarios within a limited computational time.

CONCLUSIONS

Small debris fragments can still be dangerous in case of collision as they may cause anomalies or, for fragments larger than 1 cm, even the destruction of the satellite with whom they impact. The study of the dynamics of small debris fragments requires alternative methods to the ones used for the propagation of larger objects because treating each fragment individually would result in a prohibitive computational time This work proposed a propagation method based on the continuity equation, which is able to describe the evolution of the density of a debris cloud in the (a, e) domain once the values of true anomaly, argument of the perigee and longitude of the ascending node are uniformly distributed among the fragments. This information was combined together with some analytical expressions available in the literature to estimate the relative velocity between a target and a set of objects. This approach was validated by developing a numerical procedure able to measure the distance between the target orbit and each fragment orbit; for the fragments whose distance is below a set threshold, the relative velocity with respect to the target is computed and compared with the estimation obtained by the analytical expressions. The analytical estimation of the velocity was tested with different combinations of the target and the fragmentation inclination. It was found that as the target inclination approaches 90 degrees, the accuracy of the estimation is poor; it was also shown that an alternative formulation may be able to reduce drastically the error, so future work will focus on developing a formulation robust to any choice of the inclination. For other values of the inclination the relative error between the average relative speed and the analytical estimation was found to be smaller than 10%. Finally, the cloud density obtained with the continuity equation and the analytical estimation of the average relative velocity were used to compute the collision probability for a spacecraft crossing a debris cloud. An illustrative application was shown describing the collision probability for a spacecraft crossing a cloud formed by more than 2000 fragments along three years of simulation, with a computational time equal to 140 s. Future work will exploit the reduced computational time of the proposed approach to study several collision scenarios and assess how the parameters of the fragmentation affect the collision probability for a set of targets.

ACKNOWLEDGEMENT

Camilla Colombo acknowledges the support received by the Marie Curie grant 302270 (SpaceDebECM - Space Debris Evolution, Collision risk, and Mitigation), within the 7$^{\text{th}}$ European Commu-

nity Framework Programme.

APPENDIX: VALIDATION PROCEDURE

The distance between the orbit of the target and the one of a fragment is computed starting from the output of the numerical propagation performed with a semi-analytical method, PLANODYN,[21] based on averaged Gauss' equations for the evolution of the orbital parameters.

At a certain time t, the vectors of the orbital parameters of both the objects are known. From the orbital parameters, position and velocity can easily expressed in the perifocal system, which is the reference system centred in the the Earth, with xy-plane coincident with the orbital plane and the x-axis directed towards the pericentre.[22]

The following symbols

$$(\mathbf{r})_{\text{PF,T}} \quad (\mathbf{v})_{\text{PF,T}} \quad (\mathbf{r})_{\text{PF,F}} \quad (\mathbf{v})_{\text{PF,F}}$$

are introduced to indicate the distance and the velocity of the target (T) and the fragment (F) in their respective perifocal systems. Then, a rotation matrix $\mathbf{R}$, with

$$\mathbf{R}_T = R(i_T, \omega_T, \Omega_T) \quad \mathbf{R}_F = R(i_F, \omega_F, \Omega_F),$$

can be used to transform the components of these vector in a geocentric-equatorial inertial system (GEI)[22]

$$\mathbf{r}_T = \mathbf{R}_T(\mathbf{r})_{\text{PF,T}} \quad \mathbf{v}_T = \mathbf{R}_T(\mathbf{v})_{\text{PF,T}} \quad \mathbf{r}_F = \mathbf{R}_F(\mathbf{r})_{\text{PF,F}} \quad \mathbf{v}_F = \mathbf{R}_F(\mathbf{v})_{\text{PF,F}}.$$

From these vectors it is possible to compute the angular momentum vectors ($\mathbf{h}$)

$$\mathbf{h}_T = \mathbf{r}_T \times \mathbf{v}_T \quad \mathbf{h}_F = \mathbf{r}_F \times \mathbf{v}_F$$

that are perpendicular to their respective orbital planes. The line of intersection between the two planes is found by identifying the direction perpendicular to both the normals to the plane, so in this case

$$\mathbf{n} = \mathbf{h}_T \times \mathbf{h}_F.$$

The line of intersection, or *nodal* line, $\mathbf{n}$ can be projected back to the two perifocal systems

$$(\mathbf{n})_{\text{PF,T}} = \mathbf{R}_T^{-1}\mathbf{n} \quad (\mathbf{n})_{\text{PF,F}} = \mathbf{R}_F^{-1}\mathbf{n},$$

so that the problem becomes finding, on each perifocal plane, the intersection between a line and the ellipse representing the orbit. The problem is solved considering that the points of intersection will have true anomaly equal to

$$\nu_i = \arctan\left[\frac{(n_y)_{\text{PF}}}{(n_x)_{\text{PF}}}\right] + k\pi \quad k = 0, 1$$

where $(n_x)_{\text{PF}}$ and $(n_y)_{\text{PF}}$ indicate respectively the first and the second component of the vector $(\mathbf{n})_{\text{PF,}}$. Once the true anomaly is known, the position and the velocity in the points are known too, and they can be projected to the GEI to measure the distance between the distance between the two couples of points.

REFERENCES

[1] P. H. Krisko, "The predicted growth of the low-Earth orbit space debris environment an assessment of future risk for spacecraft," *Proceedings of the Institution of Mechanical Engineers, Part G: Journal of Aerospace Engineering*, Vol. 221, Jan. 2007, pp. 975–985, 10.1243/09544100JAERO192.

[2] A. Rossi, A. Cordelli, and C. Pardini, "Modelling the space debris evolution: Two new computer codes," *Advances in the Astronautical Sciences-Space Flight Mechanics*, Apr. 1995, pp. 1–15.

[3] F. Letizia, C. Colombo, and H. G. Lewis, "Analytical model for the propagation of small debris objects after a fragmentation event," *24th AAS/AIAA Space Flight Mechanics Meeting*, Santa Fe, Jan. 2014. AAS 14-324.

[4] C. R. McInnes, "An analytical model for the catastrophic production of orbital debris," *ESA Journal*, Vol. 17, No. 4, 1993, pp. 293–305.

[5] N. L. Johnson and P. H. Krisko, "NASA's new breakup model of EVOLVE 4.0," *Advances in Space Research*, Vol. 28, No. 9, 2001, pp. 1377–1384, 10.1016/S0273-1177(01)00423-9.

[6] P. H. Krisko, "Proper Implementation of the 1998 NASA Breakup Model," *Orbital Debris Quarterly News*, Vol. 15, No. 4, 2011, pp. 1–10.

[7] D. King-Hele, *Satellite orbits in an atmosphere: theory and application*. Glasgow and London: Blackie, 1987. ISBN: 9780216922525.

[8] D. A. Vallado, *Fundamentals of astrodynamics and applications*. Springer, 4th ed., 2013. Pages 551–573, 619–688. ISBN: 978-1881883180.

[9] D. S. McKnight, "A phased approach to collision hazard analysis," *Advances in Space Research*, Vol. 10, Jan. 1990, pp. 385–388, 10.1016/0273-1177(90)90374-9.

[10] F. Letizia, C. Colombo, and H. G. Lewis, "Analytical model for the propagation of small debris objects clouds after fragmentations," *Journal of Guidance, Control, and Dynamics*, 2014. [Accepted].

[11] F. Letizia, C. Colombo, and H. G. Lewis, "Continuity equation method for debris cloud evolution," *Advances in Space Research*, 2014. [Submitted].

[12] N. Gor'kavyi, "A new approach to dynamical evolution of interplanetary dust," *The Astrophysical Journal*, Vol. 474, No. 1, 1997, pp. 496–502, 10.1086/303440.

[13] C. R. McInnes, "Simple analytic model of the long term evolution of nanosatellite constellations," *Journal of Guidance Control and Dynamics*, Vol. 23, No. 2, 2000, pp. 332–338, 10.2514/2.4527.

[14] C. Colombo and C. R. McInnes, "Evolution of swarms of smart dust spacecraft," *New Trends in Astrodynamics and Applications VI*, New York, Courant Institute of Mathematical Sciences, June 2011.

[15] J. Ashenberg, "Formulas for the phase characteristics in the problem of low-Earth-orbital debris," *Journal of Spacecraft and Rockets*, Vol. 31, Nov. 1994, pp. 1044–1049, 10.2514/3.26556.

[16] D. J. Kessler, "Derivation of the collision probability between orbiting objects: the lifetimes of Jupiter's outer moons," *Icarus*, Vol. 48, Oct. 1981, pp. 39–48, 10.1016/0019-1035(81)90151-2.

[17] F. Letizia, C. Colombo, and H. G. Lewis, "Continuity equation approach for the analysis of the collision risk due to space debris clouds generated by a fragmentation event," *International Astronautical Congress*, Toronto, Sept. 2014. IAC-14.A6.P.31.

[18] F. Letizia, C. Colombo, and H. G. Lewis, "Small debris fragments contribution to collision probability for spacecraft in Low Earth Orbit," *7th IAASS Conference*, Friedrichshafen, Oct. 2014.

[19] C. Bonanno, "An analytical approximation for the MOID and its consequences," *Astronomy and Astrophysics*, Vol. 416, 2000, pp. 411–416.

[20] A. Rossi, G. B. Valsecchi, L. Anselmo, C. Pardini, H. G. Lewis, and C. Colombo, "Fragmentation Consequence Analysis for LEO and GEO Orbits," *GreenOps Workshop*, Noordwijk, Nov. 2013. ESA AO 1/7121/12/F/MOS.

[21] C. Colombo, "Long-term evolution of highly-elliptical orbits: luni-solar perturbation effects for stability and re-entry," *25th AAS/AIAA Space Flight Mechanics Meeting*, Williamsburg, VA, Jan. 2015. AAS 15-395.

[22] R. R. Bate, D. D. Mueller, and J. E. White, *Fundamentals of astrodynamics*. Dover, 1th ed., 1971. Pages 53–57, 74–82. ISBN-13: 978-0486600611.